

# Natural grid stretching for DNS of wall-bounded flows

Sergio Pirozzoli\*, Paolo Orlandi

*Dipartimento di Ingegneria Meccanica e Aerospaziale, Sapienza Università di Roma, Via Eudossiana 18, Roma 00184, Italy*

arXiv:2104.05774v1 [physics.flu-dyn] 12 Apr 2021

---

## Abstract

We propose a natural stretching function for DNS of wall-bounded flows, which blends uniform near-wall spacing with uniform resolution in terms of Kolmogorov units in the outer wall layer. Numerical simulations of pipe flow are used to educe optimal value of the blending parameter and of the wall grid spacing which guarantee accuracy and computational efficiency as a results of maximization of the allowed time step. Conclusions are supported by DNS carried out at sufficiently high Reynolds number that a near logarithmic layer is the mean velocity profile is present. Given a target Reynolds number, we provide a definite prescription for the number of grid points and grid clustering needed to achieve accurate results with optimal exploitation of resources.

---

## 1. Introduction

Direct numerical simulation (DNS) of wall-bounded flows is by now an established practice, started from the pioneering work of Kim et al. (1987) for channel flow. Although meshing is not a challenging issue given the simple topology of canonical flows to which DNS is currently limited, the mesh parameters significantly affect computational accuracy and efficiency. It is generally acknowledged (e.g. Lee and Moser, 2015) that mesh spacings in the order of ten wall units in the streamwise direction and five in the spanwise direction are sufficient in pseudo-spectral calculations to achieve good resolution of the buffer-layer energy-containing eddies, namely streaks and associated quasi-streamwise vortices. The buffer layer is especially important as the topology of eddies changes from sheet-like near the wall to rod-like away from it, corresponding to the inflectional point of the wall-normal velocity variance profile (Orlandi, 2013). Finite-difference schemes require similar or slightly higher number of grid points (Bernardini et al., 2014), to achieve the same quality of results. More disputable is the selection of the mesh properties in the wall-normal direction, which is strongly anisotropic for the flow, and for which no rule is consolidated yet. In fact, different authors of state-of-art DNS have used vastly different mapping functions, and the selection of the total number of grid points is mainly a matter of personal experience and feeling. Another important issue in the design of modern DNS is computational efficiency. In fact, it turns out that the admissible time step is strongly affected by the wall-normal distribution of the grid points, and changing the mapping function can yield substantial saving of computer time, with little or no loss of accuracy. While some inefficiency is forgiven in small-scale DNS carried out on local

---

\*Corresponding author: Tel.: (+39) 06 44585202; fax: (+39) 06 44585250;  
Email address: [sergio.pirozzoli@uniroma1.it](mailto:sergio.pirozzoli@uniroma1.it) (Sergio Pirozzoli)

computer clusters, this is clearly not allowed in leading-edge numerical simulations exploiting huge computational resources. The purpose of this paper is to provide the community of DNS of wall-bounded flows with a tailored mapping function and definite grid point number estimates, so as to satisfy natural resolution requirements and at the same time to provide maximum computational performance. Although the forthcoming discussion is mainly focused on the case of turbulent pipe flow, other canonical cases can also be handled with no or minimum modifications, as plane channel and boundary-layer flows.

## 2. Wall-normal stretching functions

Considerations about the multi-scale nature of wall-bounded turbulence lead to conclude that several constraints shall be satisfied for effective design of the wall-normal mapping function: i) the first off-wall grid node (say  $\Delta y_w^+$ ) shall be placed close enough that the severe velocity gradients occurring in that region are resolved, which requires  $\Delta y_w^+ \lesssim 1$ ; ii) grid points should be conveniently clustered within the buffer layer (say,  $y^+ \leq 50$ ) which is the most anisotropic region of the flow, and in which most intense phenomena occur; iii) the spacing in the outer part of the wall layer, in which turbulence is not far from isotropic, should be proportionate to the local Kolmogorov length scale. Synthetic information about previous DNS studies of channel and pipe flows is provided in Table 1, where  $Re_\tau = u_\tau \delta / \nu$  (with  $u_\tau$  the friction velocity,  $\delta$  either the channel half-height or the pipe radius or the boundary layer thickness, and  $\nu$  the fluid kinematic viscosity) is the friction Reynolds number,  $N_y$  is the number of collocation points in the wall-normal direction, and  $N_{buf}$  is the number of grid points within the buffer layer. As can be seen, different studies rely on different mapping functions (see Orlandi (2000) for an overview of classical ones), different near-wall resolutions, and even very different total number of points for similar  $Re_\tau$ . In this respect it should be noted that standard spectral methods only allow for cosine stretching in the vertical direction to exploit Chebyshev transform, and alternate mappings can only be accommodated by changing the numerical treatment of the wall-normal direction. For instance, Hoyas and Jiménez (2006) used sixth-order compact differencing, whereas Lee and Moser (2015) used a B-spline collocation method. On the other hand, the finite-difference method allows use of arbitrary mappings.

We believe that, given the near universality of wall-bounded flows, a universal treatment of the stretching function is possible and appropriate. We then reason as follows. First, following considerations of Hoyas and Jiménez (2006), we believe that the grid spacing in the outer layer should be selected to be proportional to the local Kolmogorov length scale, say  $\eta$ . By definition  $\eta^+ = \varepsilon^{+^{-1/4}}$ , with  $\varepsilon$  the local dissipation rate, and  $+$  denoting wall units. Since under equilibrium conditions in the log layer  $\varepsilon^+ \sim 1/y^+$ , it follows (Jiménez, 2018) that

$$\eta^+ \approx c_\eta y^{+1/4}, \quad (1)$$

with  $c_\eta \approx 0.8$ , which is consistent with all available DNS of channel and pipe flow, as we have directly checked. Hence, the first requirement which we set is that the local grid spacing in the outer layer should be  $\Delta y^+ = \alpha \eta^+$ , with  $\alpha$  controlling adequate resolution of the dissipative eddies. The choice  $\alpha = 1.5$  yields a resolution in spectral space  $k_{max} \eta \approx 2$  (where  $k_{max} = \pi/\Delta y$  is the maximum resolved wavenumber) which is regarded to be sufficient in numerical

Flow	Reference	Stretching function	$Re_\tau$	$N_y$	$\Delta y_w^+$	$N_{buf}$	Symbol
Channel	Kim et al. (1987)	Cosine	180	64	0.05	31	×
			550	128	0.041	36	
	Hoyas and Jiménez (2006)	NA	934	192	0.031	40	
			2004	317	0.32	31	□
	Lee and Moser (2015)	Cosine/splines	182	96	0.074	48	
			544	192	0.019	56	
			1000	256	0.019	55	
			5186	768	0.50	54	○
	Lozano-Durán and Jiménez (2014)	NA	4180	540	0.32	31	
			548	192	0.06	79	
	Pirozzoli et al. (2016)	Error function	995	256	0.018	79	
			2017	384	0.26	83	
			4088	512	0.38	73	△
Pipe	Wu and Moin (2008)	NA	182	256	0.17	150	
			1142	300	0.41	69	▽
	Chin et al. (2014)	NA	180	80	0.50	NA	
			500	160	0.07	NA	
			1002	192	0.6	NA	
			2003	320	0.35	NA	
	Ahn et al. (2015)	NA	180	257	0.165	NA	
			544	279	0.176	NA	
			934	301	0.33	NA	
			3008	901	0.36	NA	
Boundary layer	Schlatter and Örlü (2010)	NA	1271	212	0.033	40	◇

Table 1: List of mesh parameters for reference DNS studies.  $\Delta y_w$  is the distance of the first off-wall node, and  $N_{buf}$  is the number of grid points within  $y^+ \leq 50$ .

simulations of isotropic turbulence (Jiménez and Wray, 1998), and similar to the resolution used in channel flow by Hoyas and Jiménez (2006). Thus, let  $j$  be the wall-normal grid index (momentarily assumed to be continuous for convenience), we require that

$$\Delta y^+ = \frac{dy^+}{dj} = \alpha c_\eta y^{+1/4}, \quad (2)$$

which upon integration yields

$$y^+(j) = \left( \frac{3}{4} \alpha c_\eta j \right)^{4/3}, \quad (3)$$

which defines the mesh stretching in the outer wall layer. Next to the wall, in the viscous sublayer the mean velocity gradient is nearly constant up to  $y^+ \approx 5$ , and use of uniform spacing is appropriate, hence

$$y^+(j) = \Delta y_w^+ \cdot j. \quad (4)$$

Whereas experience from most previous DNS suggests that a reasonable value of the wall grid spacing be  $\Delta y_w^+ \approx 0.1$ , its influence on the DNS statistics will be herein discussed. A smooth blending between the near-wall mapping (3) and the outer-layer mapping (3) is further assumed, to yield

$$y^+(j) = \frac{1}{1 + (j/j_b)^2} \left[ \Delta y_w^+ j + \left( \frac{3}{4} \alpha c_\eta j \right)^{4/3} (j/j_b)^2 \right], \quad (5)$$

where the parameter  $j_b$  defines the grid index at which transition between the near-wall and the outer mesh stretching should take place, whose choice will also be discussed in detail. Straightforward differentiation of Eqn. (5) also yields the local grid spacing,

$$\Delta y^+ = \frac{dy^+}{dj} = \frac{1}{(1 + (j/j_b)^2)^2} \left[ \left( 1 - (j/j_b)^2 \right) \Delta y_w^+ + \frac{2}{3} \left( \frac{3}{4} \alpha c_\eta \right)^{4/3} \frac{j^{7/3}}{j_b^2} \left( 5 + 2(j/j_b)^2 \right) \right]. \quad (6)$$

Evaluating Eqn. (5) at the edge of the wall layer yields the number of grid points along the vertical direction as is an implicit function of  $Re_\tau$  (as it should be), and of the stretching parameters  $j_b$ ,  $\Delta y_w^+$ ,  $\alpha$ . However, under the assumption  $j \gg 1$ , hence at sufficiently high Reynolds number that the number of points within the buffer layer becomes small compared to those in the outer layer, Eqn. (5) yields

$$Re_\tau = \left( \frac{3}{4} \alpha c_\eta N_y \right)^{4/3}, \quad (7)$$

whence the number of necessary grid points to achieve a given (large)  $Re_\tau$  can be estimated,

$$N_y = \frac{4}{3 \alpha c_\eta} Re_\tau^{3/4}, \quad (8)$$

where the nearest integer should be taken for practical purposes. Representative numbers are given in Table 2. Equation (8) is quite interesting as it suggests that the total number of grid points for DNS of wall-bounded turbulence should scale as  $N_{xyz} \sim Re_\tau^{11/4}$ , whereas common estimates suggest  $N_{xyz} \sim Re_\tau^3$ , on the grounds that the thickness of the viscous wall region determines the smallest scales throughout the wall layer (Reynolds, 1990). Available channel and pipe flow data further suggest that for  $Re_\delta \gtrsim 10^5$ ,  $Re_\tau \sim Re_\delta^{0.92-0.94}$  (where  $Re_\delta = 2u_b\delta/\nu$  is the bulk Reynolds number), thus yielding an estimated total number of grid points,  $N_{xyz} \sim Re_\delta^{2.5-2.6}$ .

$Re_\tau$	500	1000	2000	5000	10000	20000
$N_y$	140	237	399	793	1333	2242

Table 2: Estimated number of grid points in wall-normal direction for DNS of wall turbulence, according to the asymptotic formula (8)

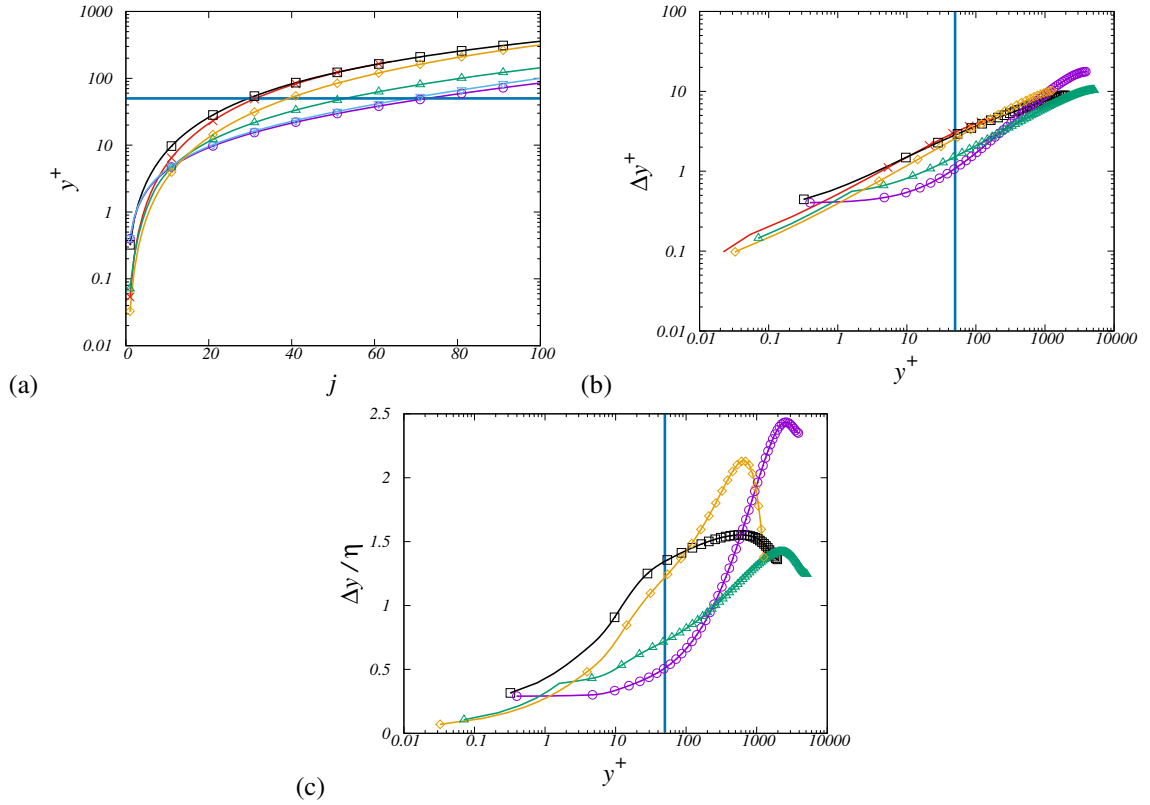


Figure 1: Mapping functions (a) and corresponding grid spacing distributions in wall units (b) and in Kolmogorov units (c) for representative DNS of wall-bounded flows. Symbols as given in Table 1. Straight horizontal and vertical lines denote the edge of the buffer layer ( $y^+ = 50$ ).

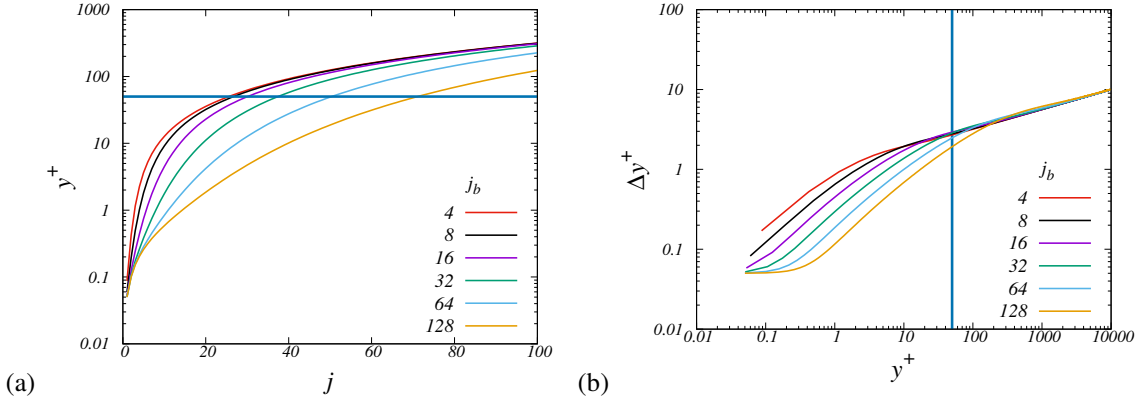


Figure 2: Mapping functions (a) and corresponding grid spacing distributions (b), according to equations (5), (6), as a function of  $j_b$ , assuming  $\Delta y_w^+ = 0.05$ ,  $\alpha = 1.25$ . Straight horizontal and vertical lines denote the edge of the buffer layer ( $y^+ = 50$ ).

The diversity of grid mappings used for DNS of wall-bounded flows is reflected in figure 1, showing the distribution of grid points for representative simulations. The mappings differ in several respects, including position of the first wall point, and number of points in the buffer layer, whose edge is marked with a horizontal line. Specifically, in the DNS of Kim et al. (1987) and Hoyas and Jiménez (2006) the grid points are more clustered towards the wall, at the expense of having limited number of points in the buffer layer, about thirty. Other DNS (Wu and Moin, 2008; Pirozzoli et al., 2016) have larger wall spacing and more points in the buffer layer, up to seventy. Other cases (Lee and Moser, 2015; Schlatter and Örlü, 2010) fall in between. This difference is appreciated in panel (b), showing the mesh spacing as a function of the wall distance. Whereas most DNS have a spacing of 2-3 wall units at the edge of the buffer layer, other have nearly uniform spacing in the viscous sublayer, and spacing of about one wall unit at the edge of the buffer layer. To have a perception for the grid resolution in the outer layer, in panel (c) we show the mesh spacing normalized by the local Kolmogorov length scale, limited to those cases in which the latter is available. The effective resolution of most DNS in the outer layer is about 1.25-1.5 Kolmogorov units, and a bit poorer in the case of the DNS of Schlatter and Örlü (2010) and Pirozzoli et al. (2016).

### 3. Numerical tests

#### 3.1. Effect of the $j_b$ parameter

The stretching functions herein designed along with the associated grid spacing distributions are shown for various  $j_b$  in figure 2, where we assume  $\Delta y_w^+ = 0.05$ ,  $\alpha = 1.25$ . As intended, the  $j_b$  parameter controls the number of grid points within the buffer layer, changing from about 25 to about 70 as  $j_b$  ranges between 4 and 128. The near-wall spacing is increasing at low  $j_b$ , whereas for all cases the grid spacing at the edge of the buffer layer is  $\Delta y^+ \approx 3$ , and  $\Delta y^+ \approx 2$  for  $j_b = 128$ . Comparison with figure 1 shows that change of  $j_b$  allows to basically cover the range of stretching functions used in previous studies.

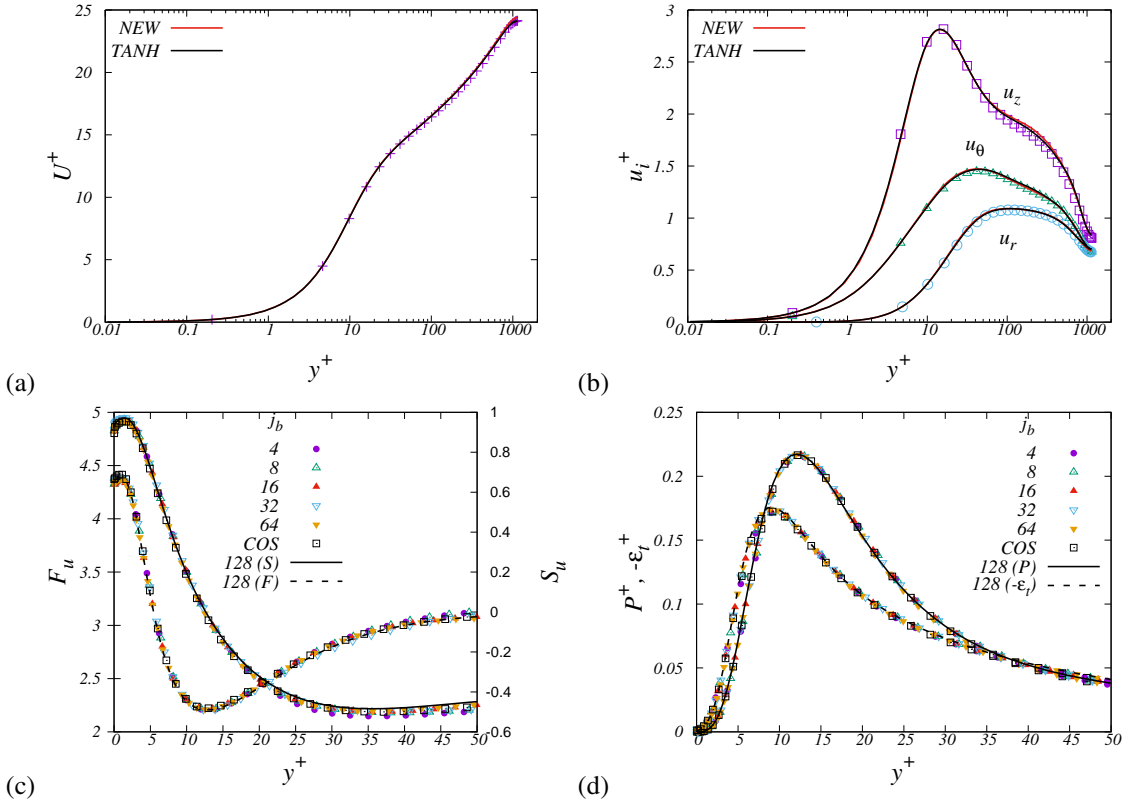


Figure 3: DNS of pipe flow at  $Re_\delta = 5300$ , effect of  $j_b$  stretching parameter: profiles of (a) mean velocity, (b) r.m.s. velocity fluctuations (axial,  $u_z$ ; wall-normal,  $u_r$ ; azimuthal,  $u_\theta$ ), (c) skewness and flatness of  $u_z$ , and (d) turbulence kinetic energy production ( $P = -\overline{u_r u_z} dU/dy$ , solid lines), and total dissipation ( $\epsilon_t = \overline{\nu u_i \nabla^2 u_i}$ , dashed lines). Symbols in panels (a, b) denote velocity statistics of Wu and Moin (2008). Lines in panels (c, d) denote numerical results obtained with  $j_b = 128$ , which are used as a reference. The square symbols denotes results obtained using the cosine stretching function, with  $N_y = 64$ .

In order to show how the choice of  $j_b$  impacts the quality of numerical results and the involved computational effort we have carried out a series of numerical experiments of pipe flow at modest Reynolds number ( $Re_\delta = 5300$ ), using a well-established solver (Verzicco and Orlandi, 1996; Orlandi and Fatica, 1997), modified with implicit treatment of the azimuthal convective terms (Akselvoll and Moin, 1996; Stevens et al., 2013). The rationale is that, since the buffer-layer dynamics is weakly affected by Reynolds number variations, the results of the analysis can be extrapolated to higher Reynolds number. In all the simulations the computational domain is 15 pipe radii long, and 256 grid points are used in the axial and azimuthal directions, with corresponding grid spacings  $\Delta x^+ \approx 10.7$ ,  $R^+ \Delta \theta = 4.5$ . In these exploratory simulations the value of  $N_y$  is varied from case to case, according to equation (5), from  $N_y = 66$  for  $j_b = 4$  to  $N_y = 116$  for  $j_b = 128$ . However, differences in the total number of points would become vanishingly small at higher  $Re$ , as reflected in the asymptotic formula (8). The resulting flow statistics are shown in figure 3, along with reference data of Wu and Moin (2008), who reported a friction Reynolds number  $Re_\tau = 181.4$ . Here, we find that  $Re_\tau$  ranges between 181.1 and 182.1 as  $j_b$  varies, hence the impact on frictional drag is less than 0.5%. The impact is also small on the main flow statistics, including inner-scaled mean velocity profiles (panel (a)) and velocity fluctuations intensities (panel (b)), although limited scatter and slight differences with respect to the reference data are visible in the axial turbulence intensity towards the pipe axis. The higher-order moments of  $u$  (panel(c)) show that lower resolution implies slight overprediction of the magnitude of skewness and flatness in the outer part of the buffer layer. Some resolution effect is observed on the distribution of the turbulence kinetic energy production rate and total dissipation rate ( $\epsilon_t = \overline{v u_i \nabla^2 u_i}$ , namely the sum of the viscous dissipation and diffusion terms), shown in panel (d). Not surprisingly, dissipation is most affected being representative of the small-scale dynamics, and we find that coarser mesh resolution in the buffer layer, i.e. lower  $j_b$ , yields reduction of peak dissipation. Specifically, assuming the case  $j_b = 128$  as a reference, we find that the underprediction is of about 2.5% for  $j_b = 4$ , 1.0% for  $j_b = 16$ , and 2.0% with the cosine stretching function. Much smaller effect is found on the production term, which is underestimated by at most 0.4% at  $j_b = 4$ , and by less than 1% when using the cosine stretching function.

Computational efficiency in the numerical simulation of wall-bounded flows is critically affected by the admissible time step. Given severe bounds placed by the viscous time step restriction, most DNS codes rely on implicit treatment of the viscous terms in all coordinate directions, or at least in the wall-normal direction (Orlandi, 2000). Treatment of the convective terms is instead typically explicit, and computations are time advanced at  $O(1)$  CFL number. A notable exception is the case of pipe flow, in which the metric singularity yields unnecessarily small time step towards the pipe axis, and implicit treatment of the convective terms, or progressive reduction of the Fourier modes towards the axis, becomes necessary (Boersma, 2011). In any case, also given that the axial time step restriction can be alleviated using a moving reference frame (Bernardini et al., 2013), the wall-normal time step restriction is typically the most restrictive, and it can be mitigated through suitable design of the stretching function. This is portrayed in figure 4(a), where we show the local convective time step restriction associated with each coordinate direction, assuming  $CFL=1$ , hence  $\Delta t_{\max,z} = \Delta z / (\max |u_z|)$  (axial, solid line),  $\Delta t_{\max,r} = \min(\Delta y / |u_r|)$  (radial, dashed lines),  $\Delta t_{\max,\theta} = \min(r \Delta \theta / |u_\theta|)$  (azimuthal, dash-dotted line). The viscous time step limitations are not shown as they can be easily by-passed by implicit time integration. Also, since the axial and azimuthal mesh spacings are not changed, only one dashed line



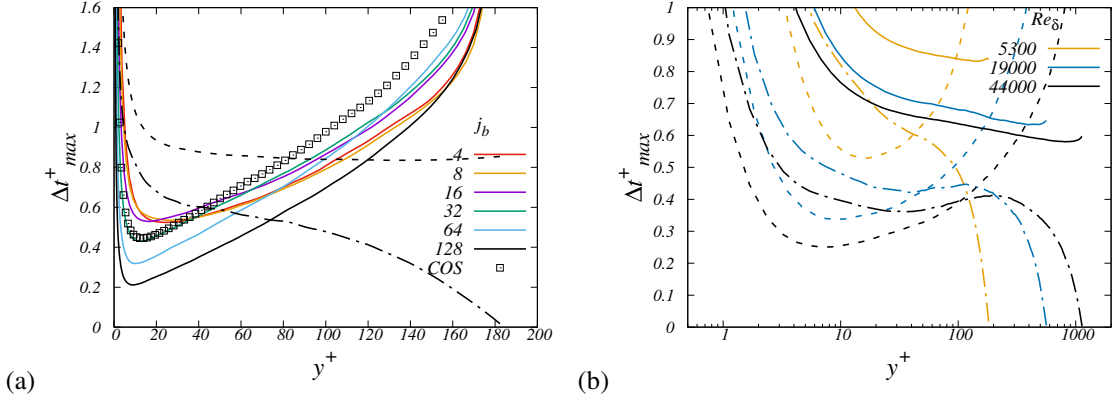


Figure 4: Time step limitations in DNS of pipe flow at  $Re_\delta = 5300$  as a function of  $j_b$  (a), and for  $j_b = 16$  at various  $Re_\delta$  (b). The line style indicates the limitation associated with each spatial direction: wall-normal (solid), axial (dashed), and azimuthal (dash-dotted). The square symbols denote results obtained using the cosine stretching function, with  $N_y = 64$ .

and one dash-dotted lines are shown. The figure confirms that the axial time step restriction is less compelling than the other (the simulation is carried out in a moving frame of reference), and the spanwise restriction becomes too demanding towards the axis, but this is disregarded in our simulations as we rely on implicit treatment of the convective terms in the  $\theta$  direction (Akselvoll and Moin, 1996). The wall-normal time step restriction (solid lines) is thus found to be the most compelling, and to depend critically on the mesh stretching through the parameter  $j_b$ , with  $\Delta t_{\max,r}^+ \approx 0.5$  for  $j_b \leq 16$ , and reducing to  $\Delta t_{\max,r}^+ \approx 0.2$ , for  $j_b = 128$ .

Given the previously noted improved resolution of the small scales at increasing  $j_b$ , it seems that a good compromise between accuracy and computational efficiency (i.e. large time step) is achieved for  $j_b = 16$ . This value is thus retained in additional tests at higher Reynolds, whose results are shown in panel (b). There, results of pipe flow DNS are reported for  $Re_\delta = 19000$  on a  $896 \times 150 \times 896$  mesh (in  $z, r, \theta$ , respectively), and at  $Re_\delta = 44000$  on a  $1792 \times 270 \times 1792$  mesh. The same qualitative behavior of the time step restriction is found at all  $Re_\delta$ , however with reduction of the inner-scaled maximum time step as a consequence of the increased intensity of vertical velocity fluctuations in the buffer layer.

### 3.2. Effect of the $\Delta y_w^+$ parameter

The effect of the wall spacing parameter  $\Delta y_w^+$ , has then been evaluated by assuming  $j_b = 16$ ,  $\alpha = 1.25$ . The resulting stretching functions and the associated grid spacing distributions are shown for various  $\Delta y_w^+$  in figure 5. Whereas the distribution of the grid points outside the buffer layer is essentially the same for all  $\Delta y_w^+$ , small values of the wall spacing parameter yield smaller spacing near the wall, and larger spacing within the buffer layer. At extreme values ( $\Delta y_w^+ > 1$ ), the grid spacing distribution may even exhibit a reversed trend with respect to the wall distance.

A series of pipe flow simulations have been carried out at  $Re_b = 5300$ , by retaining the same number of grid points in the radial direction,  $N_r = 67$ . As  $\Delta y_w^+$  varies from 0.01 to 1,  $Re_\tau$  ranges between 180.9 and 181.5, hence with scatter of less than 0.3%. Deviations become about 1% for  $\Delta y_w^+ = 5$ , with  $Re_\tau = 183.2$ . Detailed results of the grid

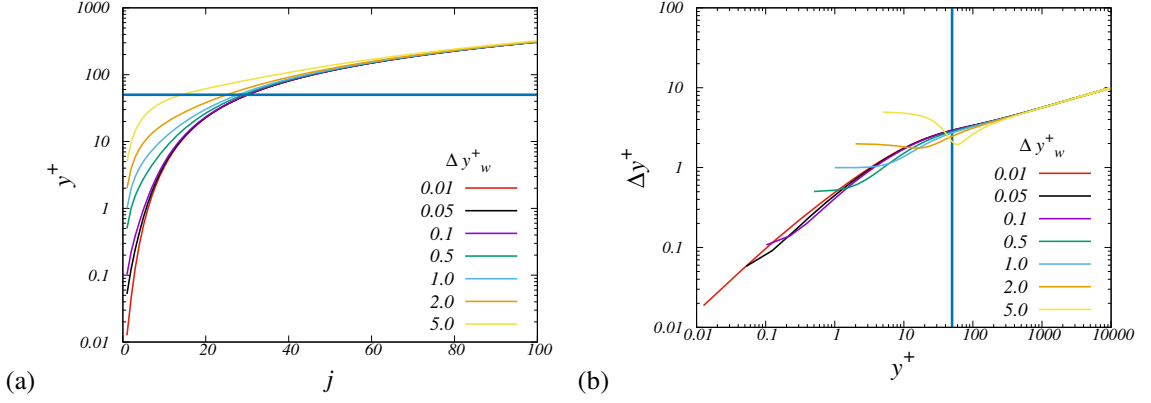


Figure 5: Mapping functions (a) and corresponding grid spacing distributions (b), according to equations (5), (6), as a function of  $\Delta y_w^+$ , assuming  $j_b = 16$ ,  $\alpha = 1.25$ . Straight horizontal and vertical lines denote the edge of the buffer layer ( $y^+ = 50$ ).

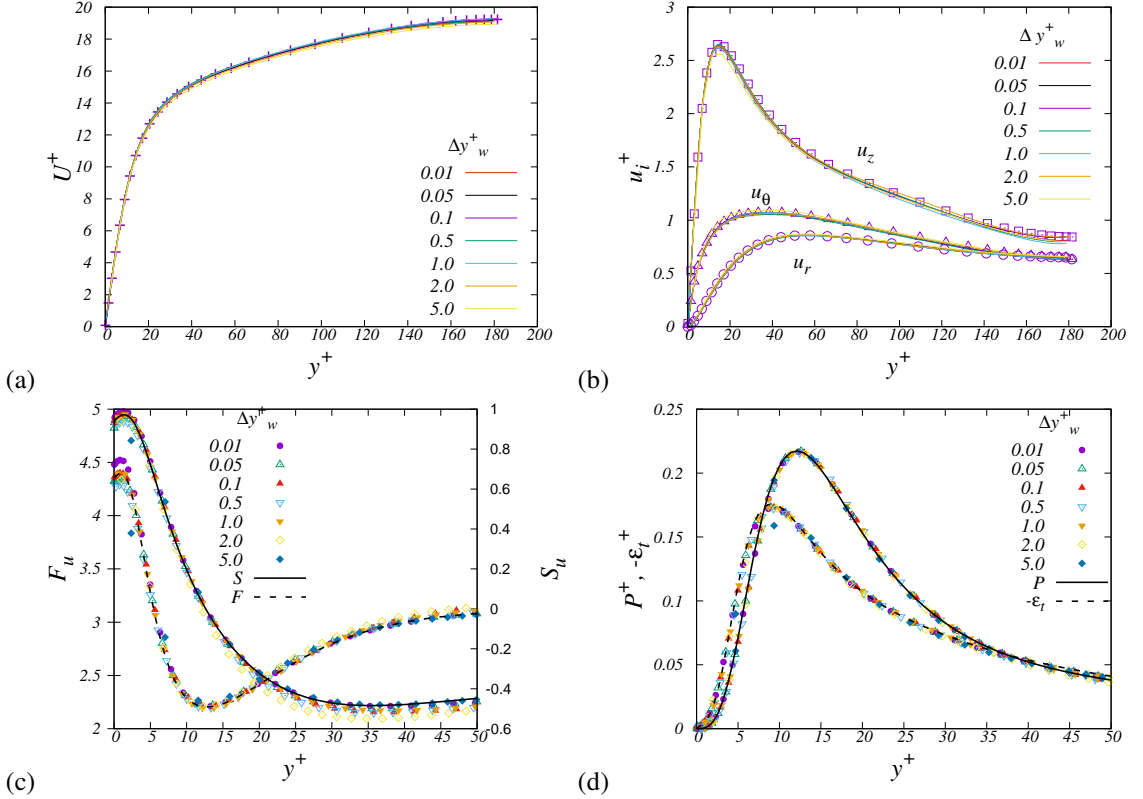


Figure 6: DNS of pipe flow at  $Re_\delta = 5300$ , effect of the  $\Delta y_w^+$  wall spacing parameter: profiles of (a) mean velocity, (b) r.m.s. velocity fluctuations (axial,  $u_z$ ; wall-normal,  $u_r$ ; azimuthal,  $u_\theta$ ), (c) skewness and flatness of  $u_z$ , and (d) turbulence kinetic energy production ( $P = -\overline{u_r u_z} dU/dy$ , solid lines), and total dissipation ( $\epsilon_t = \nu u_i \nabla^2 u_i$ , dashed lines). Symbols in panels (a), (b) denote velocity statistics of Wu and Moin (2008). Lines in panels (c), (d) denote numerical results obtained with  $j_b = 128$ ,  $\Delta y_w^+$ , which are used as a reference. The square symbols denote results obtained using the cosine stretching function, with  $N_y = 64$ .

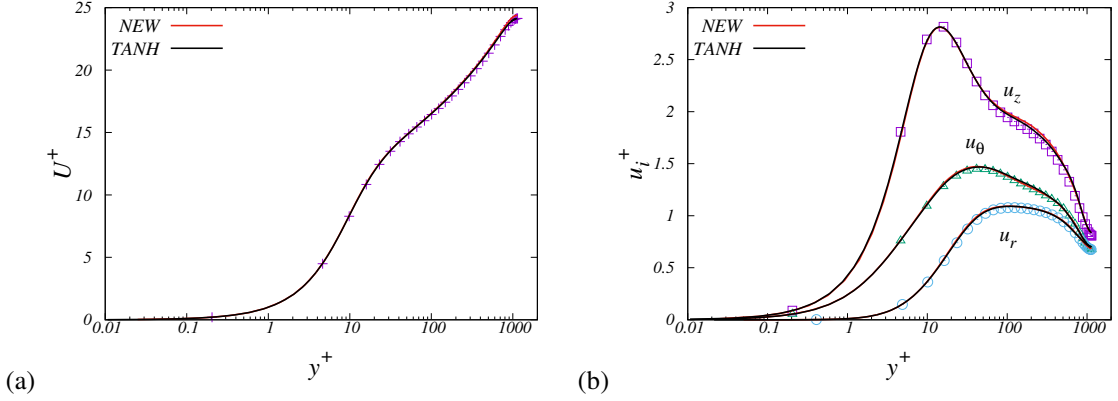


Figure 7: DNS of pipe flow at  $Re_\delta = 44000$ : profiles of (a) mean velocity and (b) r.m.s. velocity fluctuations (axial,  $u_z$ ; wall-normal,  $u_r$ ; azimuthal,  $u_\theta$ ), obtained using the new stretching function (with  $j_b = 16$ ,  $N_y = 270$ ) and a traditional hyperbolic tangent stretching function (with  $\beta = 3.8$ ,  $N_y = 512$ ). Symbols denote data of Wu and Moin (2008).

sensitivity study are shown in figure 6. The error in the mean velocity profiles (panel (a)) is limited to well less than 1% for  $\Delta y_w^+ \leq 2$ , and it is only apparent for  $\Delta y_w^+ = 5$ . The velocity variances (panel (b)) are a bit more sensitive, and some scatter in the outer layer is apparent already at  $\Delta y_w^+ = 1$ . The higher-order moments (panel (c)) are most affected by the near-wall resolution, and especially the flatness keeps increasing in the viscous sublayer as  $\Delta y_w^+$  is reduced. Far from the wall, skewness and flatness are very weakly affected, as long as  $\Delta y_w^+ \leq 1$ . Notably, the total dissipation (panel (d)) is also weakly affected by  $\Delta y_w^+$ , with the exception of the case  $\Delta y_w^+ = 5$ , which yields a reduced peak value. The maximum allowed radial time step (not shown) is barely affected for small values of the wall spacing parameter, although we find some limited gain with use of  $\Delta y_w^+ = 0.05$ , and it decreases for  $\Delta y_w^+ > 0.5$  as a result of smaller grid spacing in the buffer layer.

### 3.3. Assessment

As a final assessment of the proposed stretching function, in figure 7 we show the velocity statistics obtained at  $Re_\delta = 44000$  (yielding  $Re_\tau \approx 1140$ ) using the proposed stretching function with  $j_b = 16$ ,  $\Delta y_w^+ = 0.05$ ,  $\alpha = 1.25$ ,  $N_y = 270$ . As a basis of comparison we consider DNS results obtained with the same code, using a classical hyperbolic tangent stretching function (Orlandi, 2000), with stretching parameter  $\beta = 3.8$ , and  $N_y = 512$ , which can be regarded as a well resolved DNS. We also compare with the reference DNS results of Wu and Moin (2008). Again, no significant difference arises in the primary flow statistics, despite the vastly different distribution of grid points. On the other hand, the time step is  $\Delta t^+ = 0.22$  when using the new stretching, as compared to  $\Delta t^+ = 0.12$  when using hyperbolic tangent stretching, with clear reduction of computer time. Additional assessment of our stretching function is reported in a separate publication, in which we carry out DNS of pipe flow up to  $Re_\tau \approx 6000$  (Pirozzoli et al., 2021).

## 4. Conclusions

It is a fact that, although DNS of wall-bounded flows is by now a well established subject, the choice of the wall-normal clustering of grid points is frequently made based on subjective judgement, or based on constraints from the numerical algorithm. With the purpose of systematizing the matter, we propose a simple stretching function as given in equation (5). By construction, this mapping has the natural property of yielding precisely constant resolution in terms of the local Kolmogorov length scale in the outer part of the wall layer, where turbulence is not far from isotropic. Consistent with previous DNS, we set the resolution parameter in such a way that the grid spacing is  $\Delta y = 1.25\eta$ , although it can probably be taken a bit higher and reduce the total number of grid points. Interestingly, imposing constant resolution in Kolmogorov units implies that the number of grid points in the wall-normal direction should scale as  $Re_\tau^{3/4}$ , hence a bit milder rate than in the wall-parallel directions. The outer-layer stretching is combined with a near-wall uniformly-spaced distribution by means of a blending function which is controlled by a parameter ( $j_b$ ) which may be interpreted as the grid node index at which transition takes place, thus larger values of  $j_b$  imply a larger number of grid points within the buffer layer. Another relevant parameter is the wall grid spacing,  $\Delta y_w^+$ , controlling resolution in the viscous sublayer. We have found that the computed buffer-layer statistics at low Reynolds number are to a large extent independent of both  $j_b$  and  $\Delta y_w^+$ , with a sensitivity of  $O(1\%)$  at most for properties associated with small-scale turbulence activity as viscous dissipation.

On the other hand, the allowed computational time step is crucially affected by  $j_b$  (much less by the wall grid spacing), and compromise between accuracy and efficiency leads us to suggest  $j_b = 16$ ,  $\Delta y_w^+ = 0.05$ , as an optimal set of stretching parameters. Numerical simulations carried out for pipe flow at moderate Reynolds number ( $Re_\tau \approx 10^3$ ) support effectiveness and accuracy of the proposed stretching function at higher Reynolds number than considered in the preliminary tests. Results obtained at more extreme Reynolds number are reported elsewhere (Pirozzoli et al., 2021). Although DNS are shown here only for the case of pipe flow, we believe that the same mapping (perhaps with slight modifications) can be adapted to study channel flow and boundary layers, on account of the near-universality of wall-bounded turbulence (Monty et al., 2009). We thus trust that the proposed stretching can be profitably used as a common basis for the design of future DNS to reach and exceed the current threshold of  $Re_\tau \approx 10^4$ .

## References

- J. Kim, P. Moin, R. Moser, Turbulence statistics in fully developed channel flow at low Reynolds number, *J. Fluid Mech.* 177 (1987) 133–166.
- M. Lee, R. Moser, Direct simulation of turbulent channel flow layer up to  $Re_\tau = 5200$ , *J. Fluid Mech.* 774 (2015) 395–415.
- P. Orlandi, The importance of wall-normal Reynolds stress in turbulent rough channel flows, *Phys. Fluids* 25 (2013) 110813.

- M. Bernardini, S. Pirozzoli, P. Orlandi, Velocity statistics in turbulent channel flow up to  $Re_\tau = 4000$ , *J. Fluid Mech.* 742 (2014) 171–191.
- P. Orlandi, *Fluid flow phenomena: a numerical toolkit*, Kluwer, 2000.
- S. Hoyas, J. Jiménez, Scaling of velocity fluctuations in turbulent channels up to  $Re_\tau = 2003$ , *Phys. Fluids* 18 (2006) 011702.
- A. Lozano-Durán, J. Jiménez, Effect of the computational domain on direct simulations of turbulent channels up to  $Re_\tau = 4000$ , *Phys. Fluids* 26 (2014) 011702.
- S. Pirozzoli, M. Bernardini, P. Orlandi, Passive scalars in turbulent channel flow at high Reynolds number, *J. Fluid Mech.* 788 (2016) 614–639.
- X. Wu, P. Moin, A direct numerical simulation study on the mean velocity characteristics in turbulent pipe flow, *J. Fluid Mech.* 608 (2008) 81–112.
- C. Chin, J. Monty, A. Ooi, Reynolds number effects in DNS of pipe flow and comparison with channels and boundary layers, *Int. J. Heat Fluid Flow* 45 (2014) 33–40.
- J. Ahn, J. Lee, H. Jae, J. Lee, J.-H. Kang, H. Sung, Direct numerical simulation of a 30R long turbulent pipe flow at  $Re_\tau = 3008$ , *Phys. Fluids* 27 (2015) 065110.
- P. Schlatter, R. Örlü, Assessment of direct numerical simulation data of turbulent boundary layers, *J. Fluid Mech.* 659 (2010) 116–126.
- J. Jiménez, Coherent structures in wall-bounded turbulence, *J. Fluid Mech.* 842 (2018) P1.
- J. Jiménez, A. A. Wray, On the characteristics of vortex filaments in isotropic turbulence, *J. Fluid Mech.* 373 (1998) 255–285.
- W. Reynolds, The potential and limitations of direct and large eddy simulations, in: *Whither turbulence? Turbulence at the crossroads*, 1990, pp. 313–343.
- R. Verzicco, P. Orlandi, A finite-difference scheme for three-dimensional incompressible flows in cylindrical coordinates, *J. Comput. Phys.* 123 (1996) 402–414.
- P. Orlandi, M. Fatica, Direct simulations of turbulent flow in a pipe rotating about its axis, *J. Fluid Mech.* 343 (1997) 43–72.
- K. Akselvoll, P. Moin, An efficient method for temporal integration of the navier–stokes equations in confined axisymmetric geometries, *J. Comput. Phys.* 125 (1996) 454–463.
- R. Stevens, E. P. van der Poel, S. Grossmann, D. Lohse, The unifying theory of scaling in thermal convection: the updated prefactors, *J. Fluid Mech.* 730 (2013) 295–308.

- B. Boersma, Direct numerical simulation of turbulent pipe flow up to a Reynolds number of 61000, in: *Journal of Physics: Conference Series*, volume 318, 2011, p. 042045.
- M. Bernardini, S. Pirozzoli, M. Quadrio, P. Orlandi, Turbulent channel flow simulations in convecting reference frames, *J. Comput. Phys.* 232 (2013) 1–6.
- S. Pirozzoli, J. Romero, M. Fatica, R. Verzicco, P. Orlandi, Reynolds number trends in turbulent pipe flow: a DNS perspective, arXiv preprint arXiv:2103.13383 (2021).
- J. Monty, N. Hutchins, H. Ng, I. Marusic, M. Chong, A comparison of turbulent pipe, channel and boundary layer flows, *J. Fluid Mech.* 632 (2009) 431–442.

